

# Fluorescence-detected quick-scanning X-ray absorption spectroscopy

Adam H. Clark,<sup>a</sup> Patrick Steiger,<sup>a</sup> Benjamin Bornmann,<sup>b</sup> Stephan Hitz,<sup>a</sup>  
Ronald Frahm,<sup>b</sup> Davide Ferri<sup>a</sup> and Maarten Nachtegaal<sup>a,\*</sup>

<sup>a</sup>Paul Scherrer Institut, CH-5232 Villigen, Switzerland, and <sup>b</sup>Bergische Universität Wuppertal, D-42119 Wuppertal, Germany. \*Correspondence e-mail: maarten.nachtegaal@psi.ch

Received 14 August 2019

Accepted 19 February 2020

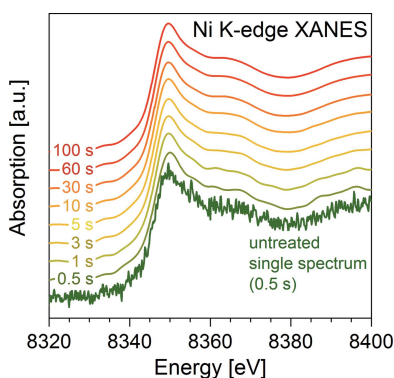
Edited by R. W. Strange, University of Essex, UK

**Keywords:** QEXAFS; fluorescence XAS; perovskite-type oxides.

Time-resolved X-ray absorption spectroscopy (XAS) offers the possibility to monitor the state of materials during chemical reactions. While this technique has been established for transmission measurements for a number of years, XAS measurements in fluorescence mode are challenging because of limitations in signal collection as well as detectors. Nevertheless, measurements in fluorescence mode are often the only option to study complex materials containing heavy matrices or in samples where the element of interest is in low concentration. Here, it has been demonstrated that high-quality quick-scanning full extended X-ray absorption fine-structure data can be readily obtained with sub-second time resolution in fluorescence mode, even for highly diluted samples. It has also been demonstrated that in challenging samples, where transmission measurements are not feasible, quick fluorescence can yield significant insight in reaction kinetics. By studying the fast high-temperature oxidation of a reduced  $\text{LaFe}_{0.8}\text{Ni}_{0.8}\text{O}_3$  perovskite type, an example where the perovskite matrix elements prevent measurements in fluorescence, it is shown that it is now possible to follow the state of Ni *in situ* at a 3 s time resolution.

## 1. Introduction

X-ray absorption spectroscopy (XAS) is a potent tool to study the oxidation state and local coordination environment of heterogeneous catalysts during operation (*operando* methodology) (Nachtegaal *et al.*, 2017). When XAS is achieved with good time resolution (10 s or better) it allows for the determination of the structure of reactive species in transient experiments (Marberger *et al.*, 2018). Both energy-dispersive XAS (Nagai *et al.*, 2008; Pascarelli *et al.*, 1999) and quick-scanning extended X-ray absorption fine-structure (QEXAFS) spectroscopy allow the collection of full EXAFS spectra in transmission mode with sub-second time resolution (Frahm, 1988; Fonda *et al.*, 2012; Müller *et al.*, 2016; Lützenkirchen-Hecht *et al.*, 2001). In previous years, QEXAFS has been mainly exploited for the collection of transmission spectra using gas-ionization chamber detectors, as these offer excellent linearity and simple adjustability of the signal intensity (Nachtegaal *et al.*, 2015). Furthermore, the introduction of gridded ionization chambers allowed one to significantly increase the response time of the ionization chambers and thus the time resolution of XAS (Müller *et al.*, 2013). There exist cases where the collection of time-resolved spectra is desirable but the material of interest does not allow the acquisition of transmission spectra. Materials with a low concentration of the element of interest and/or the presence of heavy elements, which absorb very strongly in the selected energy range, result in transmission XAS measurements not being feasible. In this case, fluorescence measurements are



desirable but present additional challenges. Since the fluorescence radiation is emitted isotropically, a large detector area is necessary to achieve high efficiency.

Multi-element solid-state detectors (SSDs), which are commonly used for fluorescence XAS measurements, suffer from low saturation count rates and low response times, which typically limit their application in time-resolved studies compared with gas-ionization chambers (Nachtegaal *et al.*, 2015). SSDs are typically limited to a count rate of several MHz when operating in photon-counting mode with modern readout electronics. For recording QEXAFS spectra, with 1 MHz counting rate from an SSD, with up to ten spectra per second and 1000 data points each, each data point would be acquired in  $\sim 100\ \mu\text{s}$  or 100 counts per point at maximum count rate, which gives a too large statistical error of 10% (based on the Poisson limit, signal-to-noise ratio  $\simeq N^{0.5}$ , where  $N$  is the number of samples at each data point). In order to achieve acceptable data quality, reducing the statistical error to 1%, count rates well in excess of 100 MHz would be required (Hansen *et al.*, 2008). Typically, experiments performed on all but very dilute samples yield a fluorescence flux in excess of  $10^6$  photons  $\text{s}^{-1}$ , which causes saturation in a SSD detector. Alternatively, avalanche photodiodes (APDs) with maximum count rates of  $\sim 100$  MHz could be used. Such systems are often used in pump-probe XAS experiments (Smolentsev *et al.*, 2018; Wang *et al.*, 2017). However, in contrast to large-area partially depleted passivated implanted planar silicon (PIPS) detectors, typically both SSDs and APDs are limited by the area of the detectors and as such the measurable solid angle of the fluorescence emitted from a sample.

Previously it has been shown that high-quality X-ray absorption near-edge structure (XANES) spectra can be recorded on a sub-second time scale using fluorescence-detected QEXAFS (Lützenkirchen-Hecht *et al.*, 2001). Elsewhere, using a highly reversible system, the application of a modulation approach to recover time resolution through repeatedly cycling the experiment at different incident X-ray energies allowed for the reconstruction of the XANES spectra with a moderate time resolution (Guda *et al.*, 2018). However, such an approach requires significant time to perform a single experiment and a full reproducibility of the chemical process. There are many cases, however, where such a time resolution is potentially of great value to enable the observation of fast irreversible processes.

Alternative methods have been employed to gain time resolution with fluorescence measurements. For instance, Turbo-XAS allows for the collection of spectra in fluorescence mode at second time resolution at energy-dispersive beamlines by scanning a slit along the energy axis of the detector (Pascarelli *et al.*, 1999). By using Turbo-XAS the redispersion of Pt on a ceria-zirconia support has been elucidated with moderate time resolution achieved for reasonable quality XANES spectra (6 s) (Nagai *et al.*, 2008). However, the Turbo-XAS method has its limitations. In particular, the limited energy bandwidth resulting from the Bragg angle variation along the incident-beam footprint on the polychromator

crystal. As a consequence, the total energy range measurable is significantly reduced at low energies (Abe *et al.*, 2018). This limitation typically makes full EXAFS data acquisition using Turbo-XAS infeasible at energies lower than  $\sim 7$  keV. Additionally, the change in direction of the slit motion results in significant dead-time between acquisitions,  $\sim 800$  ms (Pascarelli *et al.*, 1999). Furthermore, the advent of new-generation lower-emittance storage rings brings significant new challenges to energy-dispersive XAS beamlines. As a consequence of the XAS spectrum being acquired as a one-dimensional image, the larger horizontal coherence length and its negative effects on the spatial homogeneity of the beam will affect energy-dispersive XAS more than any other XAS method (Abe *et al.*, 2018).

Another method for measuring fluorescence XAS spectra with high time resolution is by means of high energy resolved off-resonant spectroscopy (HEROS) using highly resolving X-ray emission spectrometers (Szlachetko *et al.*, 2012; Błachucki *et al.*, 2014). In this case, an XAS-like spectrum is collected at one incident energy, below the resonant region of the absorption edge of interest. A dispersive emission spectrometer then allows collecting the high energy resolved XAS spectrum in a single shot (Marchionni *et al.*, 2016). However, since the X-ray cross section becomes small below the absorption edge, and the solid angle of the X-ray emission spectrometer is typically limited, this method is not applicable for dilute samples. Moreover, HEROS cannot probe the EXAFS region. Nevertheless, it is an excellent method to collect fluorescence XAS spectra free of self-absorption (Błachucki *et al.*, 2014).

Here we present the current state of fluorescence-detected XAS spectra, as can be collected at the SuperXAS beamline using a QEXAFS monochromator, with the best time resolution presented to date for the study of both dilute samples or elements in samples with a heavily absorbing matrix.

## 2. Results and discussion

For fluorescence-detected time-resolved quick-scanning XAS measurements reported herein, a PIPS fluorescence detector with an active diameter of 39 mm and a thickness of 300  $\mu\text{m}$  from Mirion Technologies has been utilized. No bias potential was applied and the capacitance of the PIPS detector used is 294 pF. The current yield from the PIPS is amplified using a very simple amplifier consisting only of the LMP7721 integrated circuit, together with a corresponding gain resistor and a tiny capacitor to limit the internal bandwidth of the chip, Fig. 1(a). The so-called trans-impedance amplifier is battery powered ( $\pm 4.5$  V) to reach the best possible signal-to-noise ratio. The internal capacitance of the PIPS detector introduces several instabilities like ringing, showing in spectra as additional oscillations behind the edge. To suppress such effects, it is therefore necessary to use a feedback capacitor. The drawback of increasing feedback capacitance results in the rise time of the amplifier chain being limited to several microseconds.

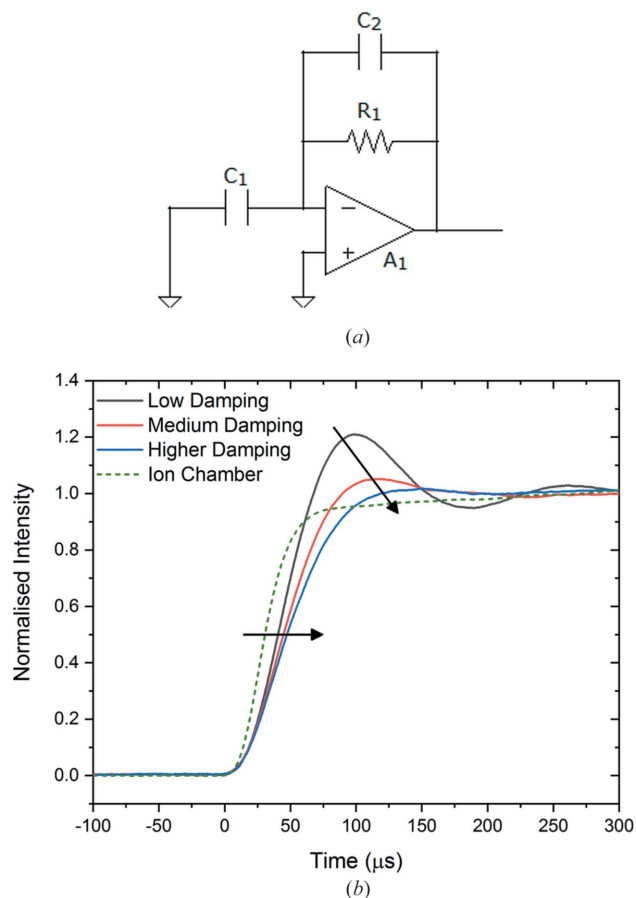


**Figure 1**

(a) Circuitry diagram for the amplifier. C1 describes the capacitance of the PIPS detector, C2 describes the feedback capacitance, R1 describes the gain resistor and A1 describes the trans-impedance amplifier. (b) The effect of increasing the feedback capacitance on the step response and rise time of the amplifier utilized and comparison with the gridded ion chamber and Keithley amplifier.

To optimize the feedback capacitance and as such reduce artefacts in measurements recorded with fast scanning through an absorption edge, the step response of the amplified PIPS signal was measured using a fast X-ray chopper rotating at 200 Hz at the SuperXAS beamline. An idealized 13 mm diameter NiO pellet (transmission edge step of 1) was mounted after the X-ray chopper and before the second ionization chamber at  $90^\circ$  to the incident X-ray beam. The PIPS detector was placed at  $\sim 30^\circ$  angle from the incident beam and facing the NiO pellet. The incident beam was tuned to 8.4 keV to yield fluorescence emission from the NiO pellet. The measurement data were recorded using a National Instruments PXIe-6366 multifunctional data-acquisition board (DAQ). The detector currents from either ion chambers or the PIPS fluorescence detector are amplified and the resulting voltages are digitized by analogue-to-digital converters of the DAQ with 16 bit resolution and sampled at 2 MHz.

The step response of the PIPS diode to incoming X-rays has a negligible rise time for QEXAFS applications but is followed by strong oscillations for several hundred microseconds when insufficiently damped. The influence of the damping with

increasing feedback capacitance is demonstrated in Fig. 1(b). Ringing of the step response is observed when insufficient feedback capacitance is used. However, increasing the feedback capacitance, whilst alleviating the ringing of the step response to the incident fluorescence, results in a slight increase in the rise time of the amplifier.

Using the optimized amplifier feedback capacitance, the sensitivity and data-collection repetition rates were explored to determine the potential useable operation limits. Three dilutions of NiO were prepared and pressed into 13 mm pellets. The mass of NiO within each pellet was estimated by consideration of the transmission XAS edge step obtained. Transmission edge steps of 0.120, 0.018 and 0.008 were observed from  $\sim 0.7$ , 0.1 and 0.05 mg of NiO diluted in cellulose. The total mass of each pellet was measured as  $\sim 50$  mg. The quick-scanning fluorescence and transmission XAS data were processed using *ProQEXAFS* (Clark *et al.*, 2020) and utilized third-order Butterworth filtering for high-frequency noise suppression. Significant signal-to-noise ratio improvements, approximately by a factor of four, are readily achievable using Butterworth filtering applied to highly oversampled XAS data (Clark *et al.*, 2020). The subsequently obtained normalized quick-scanning fluorescence XAS spectrum for each sample with a data-acquisition time of 1 s (averaging both the up and down directions) at a monochromator oscillation repetition rate of 1 Hz are shown in Fig. 2(a). Comparison between the XAS data collected in transmission geometry and in fluorescence geometry is given in Fig. 2(b) demonstrating the fluorescence XAS quality and agreement between the two measurement modes for 1 s data-acquisition periods.

The data quality achievable on such low concentrations of NiO, and in short acquisition periods (1 s), shows the versatility of the PIPS detector for time-resolved fluorescence detection XAS. Comparison of the XANES obtained at 1 Hz monochromator oscillation for the most dilute sample (transmission edge step of 0.008) for 60 s averaged spectrum and 1 s (averaged in the up and down motion of the monochromator) data-acquisition period obtained in total fluorescence yield and with 1 s in transmission geometry are shown in Fig. 3(a). It is evident that for 1 s acquisition time the data obtained in fluorescence is of a higher quality compared with the transmission data and is similar to the 60 s averaged spectra. The extraction of the EXAFS in  $k$  space and  $R$  space is given in Figs. 3(b) and 3(c), respectively. The Fourier transform window used was between 2.5 and  $10.2 \text{ \AA}^{-1}$ . From these figures, it is further evident that the transmission signal has a significantly increased noise level compared with what is achieved in total fluorescence yield with the PIPS detector. The transmission signal shows a greatly increased noise level in  $k$  space and yields an  $R$ -space pattern with significant artefacts as a result. In contrast, the 1 s and 60 s data acquisition in fluorescence demonstrate very similar profiles in both  $k$  space and  $R$  space. As such it can be noted that the 1 s data acquisition, even in the case of a very dilute sample, is not limiting the quality of the data obtainable from this sample using the PIPS detector.

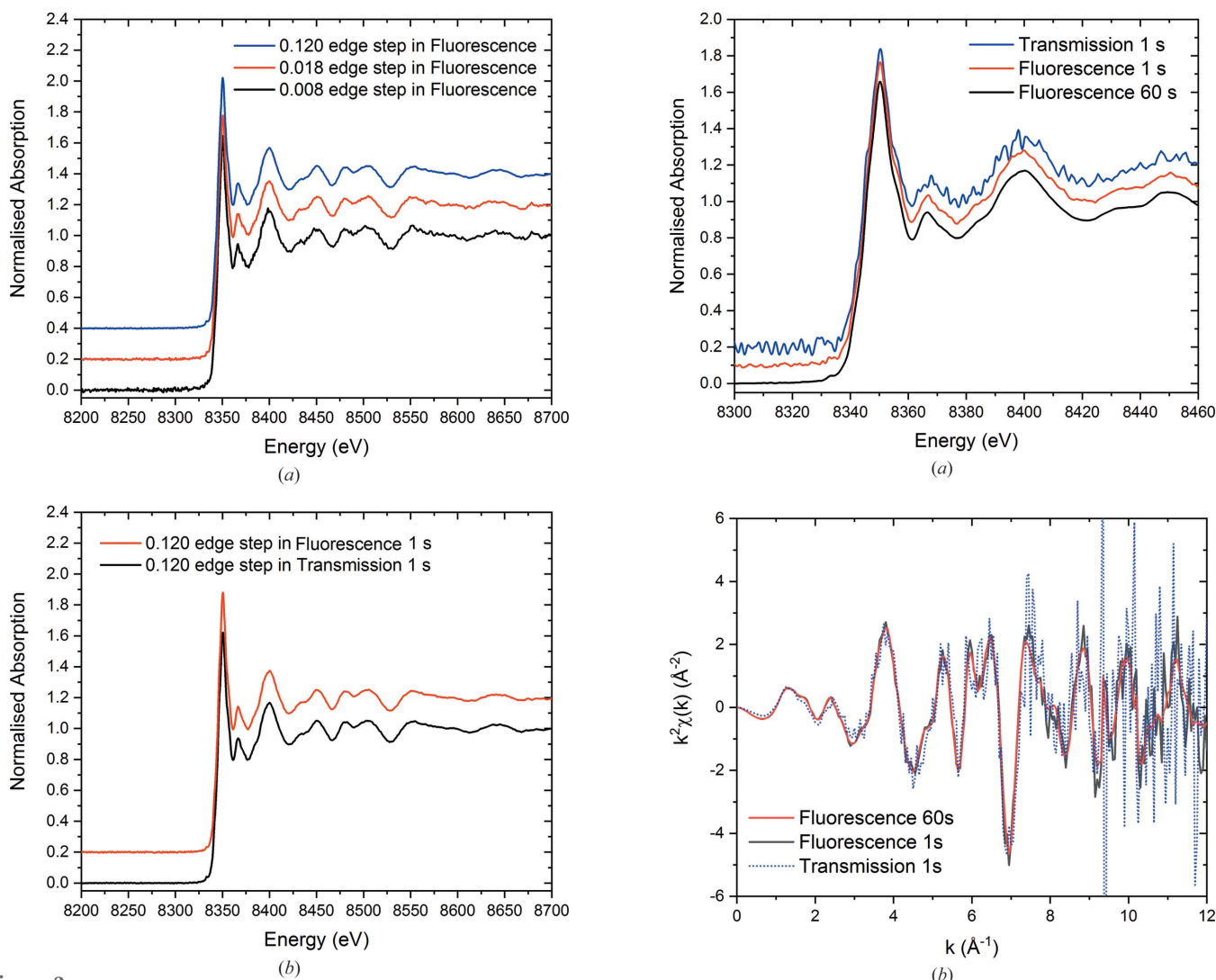


**Figure 2**  
 (a) Normalized Ni *K*-edge (8333 eV) XAS spectra measured in the fluorescence of NiO samples with decreasing sample mass pressed into 13 mm pellets. The absorption-edge step from each sample was measured from the transmission geometry data. (b) Comparison of the normalized XAS spectra obtained in 1 s for the 0.120 edge-step NiO pellet obtained in transmission and fluorescence modes.

To explore the effect of the data-acquisition period on the quality of the data obtainable in fluorescence detection, increasing monochromator oscillation frequency from 1 Hz to 10 Hz has been undertaken. Fig. 4(a) gives the XANES region of the very dilute NiO sample with increasing monochromator oscillation frequency. The data plotted are the average of 60 s data acquisition at each oscillation frequency. With increasing monochromator oscillation frequency, slight distortions in the XANES region are observed. Higher monochromator oscillation frequencies lead to a smoothing effect as a result of the finite rise time of the amplifier used. As such using the PIPS detector with monochromator oscillation frequencies in excess of 1 Hz should be carried out with care. However, for following trends in oxidation-state changes and speciation changes during reactive chemistry, the resolution on the XANES is still sufficient even at 10 Hz. Fig. 4(b) gives the

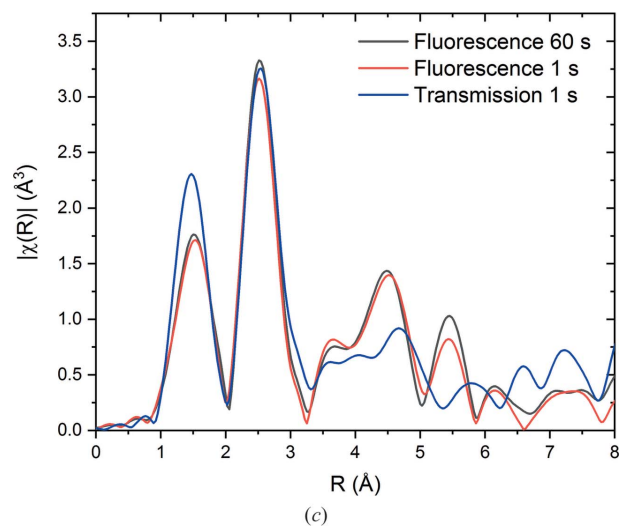


**Figure 3**  
 Normalized Ni *K* edge (8333 eV) XAS data of a very dilute NiO sample comparing the 1 s transmission (0.008 edge step), 1 s fluorescence detection and 60 s averaged fluorescence in blue, red and black, respectively. The XANES region,  $k^2$ -weighted  $k$  space and  $R$ -space spectra are shown in (a), (b) and (c), respectively.



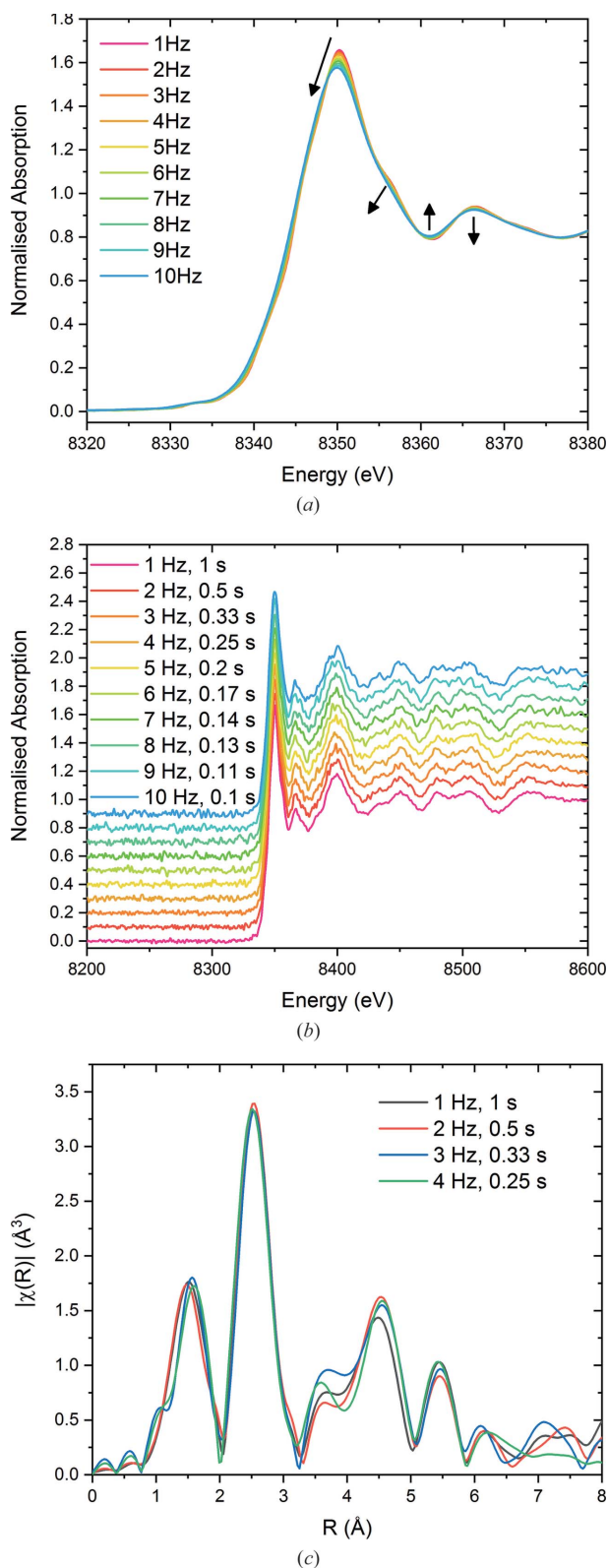


**Figure 4**  
 (a) Normalized Ni *K*-edge (8333 eV) XANES data measured in fluorescence of a very dilute NiO sample (0.008 edge step), comparing a 60 s averaged data-acquisition period for increasing monochromator oscillation frequency. (b) A stacked plot of the extended XAS data collected with increasing monochromator oscillation frequency and decreased total signal-acquisition period. (c) Obtained *R*-space data of 1 to 0.25 s data-acquisition periods.

average of the up and down spectra acquired at each monochromator oscillation frequency corresponding to 1 to 0.1 s data-acquisition periods from 1 to 10 Hz. Here it is demonstrated that even at very short data-acquisition periods the quality of the obtainable data is still outstanding considering the high dilution (transmission edge step of 0.008) of the NiO sample. Whilst transmission data could not yield high enough quality for the EXAFS region on this sample, useable quality EXAFS data are obtained from the PIPS detector with even 4 Hz monochromator oscillation frequency (0.25 s data acquisition), Fig. 4(c). The noise level at frequencies higher than 4 Hz did not allow for the Fourier transformation to *R* space between 2.5 and 10.2 Å<sup>-1</sup> to give reliable data from the very dilute NiO sample investigated (0.008 edge step).

Being able to measure time-resolved XAS spectra in fluorescence mode has obvious advantages. For the study of dilute materials, where transmission XAS no longer yields useable data, we have demonstrated that fluorescence XAS spectra can be acquired with 0.1 s time resolution for XANES and 0.25 s for EXAFS. Another class of materials which are otherwise not measurable in transmission can also significantly benefit from quick fluorescence data acquisition. One example involves the study of perovskite-type oxides (ABO<sub>3</sub>) (Peña & Fierro, 2001) where obtaining XAS of dopant elements substituting the B-site transition metal is often challenging. The heavy A-site element (lanthanide, alkali or Earth alkali element) typically absorbs very strongly at the lower energies needed to probe the local environment of the catalytically active B-site elements. As such, transmission measurements become infeasible because of the total absorption of the X-ray beam by the sample with a typical quantity of material used in *operando* XAS experiments.

Perovskites have attracted great attention in recent years for their application as active materials in electrochemical cells (*e.g.* electrolyzers, solid oxide fuel cells) (Sapountzi *et al.*, 2017; Jiang, 2008; Neagu *et al.*, 2015; Fabbri *et al.*, 2017). They have also received attention in classical heterogeneous catalysis in part because of their ability to reversibly segregate their B-site elements to produce active metal nanoparticles at the oxide surface during reduction and reincorporate these elements back into their structure during reoxidation (Nishihata *et al.*, 2002; Steiger *et al.*, 2017; Onn *et al.*, 2018). This so-called structural reversibility allows for the generation of redox stable and regenerable metal catalysts (Steiger *et al.*, 2018). Here we demonstrate the combination of fluorescence QEXAFS, which enables the speciation of Ni in LaFe<sub>0.8</sub>Ni<sub>0.2</sub>O<sub>3</sub> (4.8 wt% Ni) using fluorescence QEXAFS at the Ni *K* edge (8333 eV), and the *in situ* observation of Ni reincorporation during reoxidation at 650°C at a time resolution of 3 s.

Fig. 5 displays XANES spectra of LaFe<sub>0.8</sub>Ni<sub>0.2</sub>O<sub>3</sub> collected around the Ni *K* edge (8333 eV) in fluorescence mode for a single spectrum and averaged data. Because of the strongly absorbing nature of the perovskite there is no transmission through the sample. The spectra were collected at 1 Hz and the fluorescence signal was recorded with a 2 MHz sampling frequency and processed using *ProQEXAFS* (Clark *et al.*,

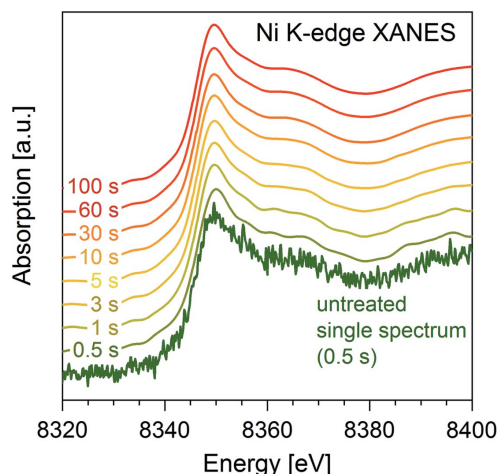


**Figure 5**  
Normalized Ni *K*-edge (8333 eV) XANES spectra of the calcined  $\text{LaFe}_{0.8}\text{Ni}_{0.2}\text{O}_3$  perovskite-type oxide for different averaging times (1–100 s). The quality of a normalized single raw spectrum (untreated, 0.5 s) and the same spectrum after noise filtering (0.5 s) are shown for comparison.

2020). Suppression of high-frequency noise was achieved using a third-order Butterworth filter in combination with a weak moving time-frame Savitzky–Golay filter. The Butterworth filter is a smooth and continuous low-pass filter allowing for the removal of high-frequency noise signals. Through this procedure it is possible to achieve a temporal resolution of at least 3 s for the XANES region. Averaging over longer times (10–100 s) did not further improve the quality of the XANES, as shown in Fig. 5. Therefore, we demonstrate that time resolutions in the second range can also be achieved on challenging materials, such as the perovskite-type oxides presented here, using the PIPS fluorescence detector and the continuous signal readout applied in this work. The time resolution achievable in this case is lower than what was possible in the dilute NiO pellet because of the significant background fluorescence from La and Fe within the perovskite sample.

The possibilities offered by using the appropriate instrumentation and data-processing methods were exploited to observe *in situ* the reincorporation of Ni metal back into the perovskite-type lattice of  $\text{LaFe}_{0.8}\text{Ni}_{0.2}\text{O}_3$  during reoxidation in 20 vol%  $\text{O}_2/\text{N}_2$  at 650°C. This process is known to occur in some pre-reduced perovskite-type oxides at sufficiently high temperatures. Furthermore, this process is known to be essential for the observed redox stability of the catalyst and can be exploited to oxidatively regenerate the catalyst from poisoning species (Steiger *et al.*, 2018, 2017; Burnat *et al.*, 2016). Prior to the experiment,  $\text{LaFe}_{0.8}\text{Ni}_{0.2}\text{O}_3$  was reduced (10 vol%  $\text{H}_2/\text{Ar}$ , 600°C, 1 h), which is known to cause the preferential reduction and segregation of metallic Ni from  $\text{LaFe}_{0.8}\text{Ni}_{0.2}\text{O}_3$  leading to the formation of metallic Ni particles on the surface of the Ni-depleted perovskite crystallites. With the

methodological advancements presented in this work it is now possible to follow such transient changes in the state of Ni *in situ* at suitable time resolutions. Fig. 6(a) displays the results of Ni speciation by linear combination analysis using the spectra of Ni in the perovskite octahedral coordination of  $\text{LaFe}_{0.8}\text{Ni}_{0.2}\text{O}_3$  ( $\text{Ni}_{\text{oct}}^{n+}$ ,  $n > 2$ ) (Steiger *et al.*, 2017) and of metallic Ni ( $\text{Ni}^0$ ) and NiO reference spectra [Fig. 6(b)]. Upon subjecting reduced  $\text{LaFe}_{0.8}\text{Ni}_{0.2}\text{O}_3$  to the oxidizing feed at 650°C,  $\text{Ni}^0$  is oxidized simultaneously to  $\text{Ni}_{\text{oct}}^{n+}$  and NiO species in the first 10–15 s. Within this time,  $\text{Ni}^0$  vanishes completely. The fraction of NiO passes through a maximum at 24 s before decreasing continuously, while the concentration of  $\text{Ni}_{\text{oct}}^{n+}$  species increases steadily. After  $\sim 1$  h all Ni has been reincorporated back into the *B* site of the perovskite lattice. At this point, the octahedral coordination environment of Ni is identical to that obtained after synthesis and its absorption spectrum resembles that observed for  $\text{LaFe}_{0.8}\text{Ni}_{0.2}\text{O}_3$  [Fig. 6(b)]. Acquisition times of a single spectrum with previously applied methods of collecting the fluorescence signal using slow energy scanning and silicon drift detectors were in the range of  $\sim 10$  min, which limited the observation of transient processes with faster kinetics significantly.

Further improvements can be made to the detection system by increasing the solid angle of the fluorescence detection, either by increasing the detector area or through the use of multiple detectors to enhance the collected fluorescence signal per time and therefore the potential time resolution. Nevertheless, these results demonstrate that it is possible with the current technology to achieve respectable time resolution through fluorescence detection *in situ* QEXAFS, and on challenging samples, and elucidate previously unresolvable time-dependent processes with application of the methodology presented in this work.

### 3. Experimental

$\text{LaFe}_{0.8}\text{Ni}_{0.2}\text{O}_3$  was prepared via the amorphous citrate process (Marcilly *et al.*, 1970) using  $\text{La}(\text{NO}_3)_3 \cdot 6\text{H}_2\text{O}$  (Sigma-Aldrich, 99.999% trace-metals basis),  $\text{Fe}(\text{NO}_3)_3 \cdot 9\text{H}_2\text{O}$  (Sigma-Aldrich,  $\geq 99.95\%$  trace-metals basis),  $\text{Ni}(\text{NO}_3)_2 \cdot 6\text{H}_2\text{O}$  (Sigma-Aldrich, 99.999% trace-metals basis) and citric acid (Sigma-Aldrich, ACS reagent,  $\geq 99.5\%$ ). The precursor

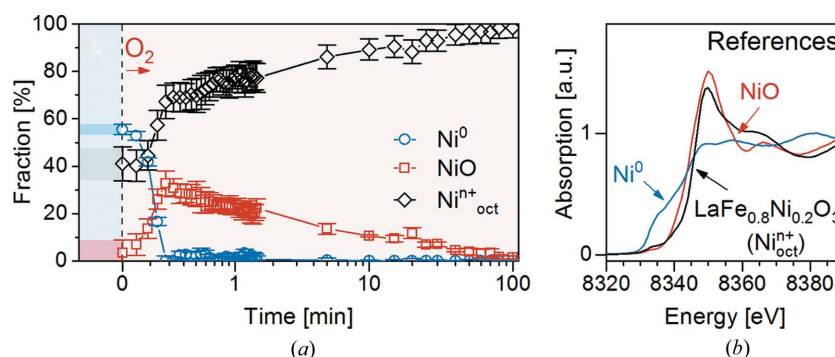


**Figure 6**  
(a) Time-resolved *in situ* Ni speciation obtained through linear combination fitting during reoxidation of pre-reduced  $\text{LaFe}_{0.8}\text{Ni}_{0.2}\text{O}_3$  at 650°C in 20 vol%  $\text{O}_2/\text{Ar}$ . (b) Ni *K*-edge XANES spectra of reference components used for linear combination fitting.

was calcined at 700°C for 2 h after drying (70°C, 12 h) to obtain the perovskite-type mixed oxide. Extensive material characterization has already been reported elsewhere (Steiger *et al.*, 2017, 2018). Ni *K*-edge (8333 eV) XAS data were collected at beamline X10DA (SuperXAS) of the Swiss Light Source (SLS, Villigen, Switzerland). The beam energy and beam current within the storage ring were 2.4 GeV and 400 mA, respectively. XAS spectra were collected in fluorescence mode using an ionization chamber filled with N<sub>2</sub> to measure incoming beam intensity and a PIPS detector mounted at 90° to the incoming X-ray beam and the sample mounted at 45°. The beam was collimated using a Si-coated mirror, which was also used for the reduction of higher harmonic contributions while the X-ray energy was continuously scanned around the Ni *K* edge using a Si (111) channel-cut monochromator at a monochromator oscillation frequency of 1 Hz (Müller *et al.*, 2016). The beam was focused to a spot size of 1.0 mm × 0.2 mm (height × width) using an Rh-coated toroidal mirror. Measurements were performed on powder samples mounted inside a quartz capillary (Hilgenberg, outer diameter 3.0 mm/inner diameter 2.9 mm). Gas flow was controlled during *in situ* measurements using mass-flow controllers (Bronkhorst) and heating provided using a hot-air blower (Leister). The sample temperature was monitored using a 0.5 mm *K*-type thermocouple placed in the centre of the sample bed. The data treatment was performed using in-house developed *ProQEXAFS* software (Clark *et al.*, 2020). Calibration of the monochromator angle to energy of the incident X-ray beam was performed through measurement of an Ni foil. Prior to normalization, the data were filtered for high-frequency noise with a Butterworth filter and the application of a weak Savitzky–Golay moving time point smoothing (window size, five spectra). Edge-step normalization was performed using a first-order polynomial and Victoreen function in the pre-edge and post-edge regions after the time-frame averaging. The data were then interpolated onto an energy grid with 0.25 eV steps in the XANES region and 0.025 Å<sup>-1</sup> steps in the EXAFS region. Ni speciation was performed through linear combination analysis of the treated spectra using reference spectra of LaFe<sub>0.8</sub>Ni<sub>0.2</sub>O<sub>3</sub>, NiO and metallic Ni. The *Demeter* software package (version 0.9.24) was used for linear combination fitting of the normalized spectra within the energy range 8.313–8.363 keV (Ravel & Newville, 2005).

### Acknowledgements

The authors are grateful for the provision of beam time by the SLS. The work was conducted as part of the Swiss Competence Center for Energy Research (SCCER BIOSWEET) of the Swiss Innovation Agency (Innosuisse).

### Funding information

The Swiss National Science Foundation (SNF, No. 200021\_159568) and the Competence Center for Energy and

Mobility (CCEM) are acknowledged for their financial support.

### References

- Abe, H., Aquilanti, G., Boada, R., Bunker, B., Glatzel, P., Nachttegaal, M. & Pascarelli, S. (2018). *J. Synchrotron Rad.* **25**, 972–980.
- Błachucki, W., Szlachetko, J., Hoszowska, J., Dousse, J. C., Kayser, Y., Nachttegaal, M. & Sá, J. (2014). *Phys. Rev. Lett.* **112**, 173003.
- Burnat, D., Kontic, R., Holzer, L., Steiger, P., Ferri, D. & Heel, A. (2016). *J. Mater. Chem. A*, **4**, 11939–11948.
- Clark, A. H., Imbao, J., Frahm, R. & Nachttegaal, M. (2020). *J. Synchrotron Rad.* **27**, 551–557.
- Fabbri, E., Nachttegaal, M., Binninger, T., Cheng, X., Kim, B. J., Durst, J., Bozza, F., Graule, T., Schäublin, R., Wiles, L., Pertoso, M., Danilovic, N., Ayers, K. E. & Schmidt, T. J. (2017). *Nat. Mater.* **16**, 925–931.
- Fonda, E., Rochet, A., Ribbens, M., Barthe, L., Belin, S. & Briois, V. (2012). *J. Synchrotron Rad.* **19**, 417–424.
- Frahm, R. (1988). *Nucl. Instrum. Methods Phys. Res. A*, **270**, 578–581.
- Guda, A. A., Bugaev, A. L., Kopelent, R., Braglia, L., Soldatov, A. V., Nachttegaal, M., Safonova, O. V. & Smolentsev, G. (2018). *J. Synchrotron Rad.* **25**, 989–997.
- Hansen, K., Reckleben, C., Diehl, I. & Klär, H. (2008). *Nucl. Instrum. Methods Phys. Res. A*, **589**, 250–258.
- Jiang, S. P. (2008). *J. Mater. Sci.* **43**, 6799–6833.
- Lützenkirchen-Hecht, D., Grundmann, S. & Frahm, R. (2001). *J. Synchrotron Rad.* **8**, 6–9.
- Marberger, A., Petrov, A. W., Steiger, P., Elsener, M., Kröcher, O., Nachttegaal, M. & Ferri, D. (2018). *Nat. Catal.* **1**, 221–227.
- Marchionni, V., Szlachetko, J., Nachttegaal, M., Kambolis, A., Kröcher, O. & Ferri, D. (2016). *Phys. Chem. Chem. Phys.* **18**, 29268–29277.
- Marcellly, C., Courty, P. & Delmon, B. (1970). *J. Am. Ceram. Soc.* **53**, 56–57.
- Müller, O., Nachttegaal, M., Just, J., Lützenkirchen-Hecht, D. & Frahm, R. (2016). *J. Synchrotron Rad.* **23**, 260–266.
- Müller, O., Stötzel, J., Lützenkirchen-Hecht, D. & Frahm, R. (2013). *J. Phys. Conf. Ser.* **425**, 092010.
- Nachttegaal, M., Hartfelder, U. & Van Bokhoven, J. A. (2017). *Springer Series in Chemical Physics*, Vol. 114, pp. 89–110. New York: Springer.
- Nachttegaal, M., Müller, O., König, C. & Frahm, R. (2015). *X-ray Absorption and X-ray Emission Spectroscopy: Theory and Applications*, Vols. 1–2, pp. 155–183. Chichester, UK: John Wiley & Sons Ltd.
- Nagai, Y., Dohmae, K., Ikeda, Y., Takagi, N., Tanabe, T., Hara, N., Guilera, G., Pascarelli, S., Newton, M. A., Kuno, O., Jiang, H., Shinjoh, H. & Matsumoto, S. (2008). *Angew. Chem. Int. Ed.* **47**, 9303–9306.
- Neagu, D., Oh, T. S., Miller, D. N., Ménard, H., Bukhari, S. M., Gamble, S. R., Gorte, R. J., Vohs, J. M. & Irvine, J. T. S. (2015). *Nat. Commun.* **6**, 8120.
- Nishihata, Y., Mizuki, J., Akao, T., Tanaka, H., Uenishi, M., Kimura, M., Okamoto, T. & Hamada, N. (2002). *Nature*, **418**, 164–167.
- Onn, T. M., Monai, M., Dai, S., Fonda, E., Montini, T., Pan, X., Graham, G. W., Fornasiero, P. & Gorte, R. J. (2018). *J. Am. Chem. Soc.* **140**, 4841–4848.
- Pascarelli, S., Neisius, T. & De Panfilis, S. (1999). *J. Synchrotron Rad.* **6**, 1044–1050.
- Peña, M. A. & Fierro, J. L. G. (2001). *Chem. Rev.* **101**, 1981–2018.
- Ravel, B. & Newville, M. (2005). *J. Synchrotron Rad.* **12**, 537–541.
- Sapountzi, F. M., Gracia, J. M., Weststrate, C. J., Fredriksson, H. O. A. & Niemantsverdriet, J. W. (2017). *Prog. Energy Combust. Sci.* **58**, 1–35.

- Smolentsev, G., van Vliet, K. M., Azzaroli, N., van Bokhoven, J. A., Brouwer, A. M., de Bruin, B., Nachtegaal, M. & Tromp, M. (2018). *Photochem. Photobiol. Sci.* **17**, 896–902.
- Steiger, P., Delmelle, R., Foppiano, D., Holzer, L., Heel, A., Nachtegaal, M., Kröcher, O. & Ferri, D. (2017). *ChemSusChem*, **10**, 2505–2517.
- Steiger, P., Nachtegaal, M., Kröcher, O. & Ferri, D. (2018). *ChemCatChem*, **10**, 4456–4464.
- Szlachetko, J., Nachtegaal, M., de Boni, E., Willmann, M., Safonova, O., Sa, J., Smolentsev, G., Szlachetko, M., van Bokhoven, J. A., Dousse, J. C., Hozowska, J., Kayser, Y., Jagodzinski, P., Bergamaschi, A., Schmitt, B., David, C. & Lücke, A. (2012). *Rev. Sci. Instrum.* **83**, 103105.
- Wang, H., Yu, C., Wei, X., Gao, Z., Xu, G.-L., Sun, D.-R., Li, Z., Zhou, Y., Li, Q.-J., Zhang, B.-B., Xu, J.-Q., Wang, L., Zhang, Y., Tan, Y.-L. & Tao, Y. (2017). *J. Synchrotron Rad.* **24**, 667–673.